LEVEL IV

AD-E410 174

(14) SBIE

(9) TECHNICAL REPORT ARCSL-TR-79050

(6) THE NATURE OF GUN SMOKE AND DUST OBSCURATION DUE TO CANNON FIRING


by

(10) Edward W. Stuebing

Emmanuel A. Lucia

Frank D. Verderame

James J. Pinto

Robert W. Doherty

SP4 George Vinansky

Research Division




(11) July 1979

(12) 35p.

(16) 1T161102A71A


US ARMY ARMAMENT RESEARCH AND DEVELOPMENT COMMAND

Chemical Systems Laboratory

Aberdeen Proving Ground, Maryland 21010




410 174

## Disclaimer



## Disposition

UNCLASSIFIED
SECURITY CLASSIFICATION OF THIS PAGE (When Data Entered)

| REPORT DOCUMENTATION PAGE | | READ INSTRUCTIONS BEFORE COMPLETING FORM |
|---|---|---|
| 1. REPORT NUMBER<br>ARCSL-TR-79050 | 2. GOVT ACCESSION NO. | 3. RECIPIENT'S CATALOG NUMBER |
| 4. TITLE (and Subtitle)<br>THE NATURE OF GUN SMOKE AND DUST OBSCURATION DUE TO CANNON FIRING | | 5. TYPE OF REPORT & PERIOD COVERED<br>Technical Report<br>August 1977<br>6. PERFORMING ORG. REPORT NUMBER |
| 7. AUTHOR(s)<br>E. W. Stuebing J. J. Pinto<br>E. A. Lucia R. W. Doherty<br>F. D. Verderame SP4 G. Vinansky | | 8. CONTRACT OR GRANT NUMBER(s) |
| 9. PERFORMING ORGANIZATION NAME AND ADDRESS<br>Commander/Director, Chemical Systems Laboratory<br>Attn: DRDAR-CLB-PS<br>Aberdeen Proving Ground, Maryland 21010 | | 10. PROGRAM ELEMENT, PROJECT, TASK AREA & WORK UNIT NUMBERS<br>1T161102A71A<br>Scientific Area 5 |
| 11. CONTROLLING OFFICE NAME AND ADDRESS<br>Commander/Director, Chemical Systems Laboratory<br>Attn: DRDAR-CLJ-R<br>Aberdeen Proving Ground, Maryland 21010 | | 12. REPORT DATE<br>July 1979<br>13. NUMBER OF PAGES<br>37 |
| 14. MONITORING AGENCY NAME & ADDRESS(If different from Controlling Office) | | 15. SECURITY CLASS. (of this report)<br>UNCLASSIFIED<br>15a. DECLASSIFICATION/DOWNGRADING SCHEDULE<br>NA |

16. DISTRIBUTION STATEMENT (of this Report)

Approved for public release; distribution unlimited.

17. DISTRIBUTION STATEMENT (of the abstract entered in Block 20, if different from Report)

18. SUPPLEMENTARY NOTES

Publication of this report was sponsored by the Army Smoke Research Program, Chemical Systems Laboratory, Aberdeen Proving Ground, Maryland. The study was conducted at Pitman-Dunn Laboratory, Frankford Arsenal under sponsorship of the Fire Control Program, but was unpublished due to closure of that laboratory.

19. KEY WORDS (Continue on reverse side if necessary and identify by block number)

| | | |
|---|---|---|
| Gunsmoke | Dust | Aerosols |
| Obscuration | Fire control | Visible |
| Near IR infrared | | |

20. ABSTRACT (Continue on reverse side if necessary and identify by block number)

Fire control systems must contend with maintaining target visibility during firing. In addition, sophisticated future fire control systems have been proposed which provide an optical guidance link to the projectile, or track a fired projectile along its trajectory and sense the miss distance at the target for automatic correction. To be successful, these systems must be able to optically track the projectile during the first few seconds after firing, during which time the transparency of the atmosphere near the muzzle is very seriously degraded by ~~gun gases~~, gun smoke, and dust
(continued on reverse side)

DD FORM 1 JAN 73 1473 EDITION OF 1 NOV 65 IS OBSOLETE

UNCLASSIFIED
SECURITY CLASSIFICATION OF THIS PAGE (When Data Entered)

20. ABSTRACT (Continued)

clouds created from the ground by muzzle blast. This paper presents an analysis of optical transmission data in three wavelength regions (visible, near IR, and far IR) collected for single shot firing of a Rarden 30 mm cannon. Spectroscopic and light scattering techniques are used to identify muzzle gas and aerosol components, and a quantitative model is constructed using Mie scattering calculations to identify equivalent monodisperse aerosols for the smoke and dust. Concentrations of ammonia gas from the muzzle emission which produce significant extinction in the 10.6$\mu$m spectral region are identified and their dissipation with time is followed. Aerosol obscuration effects are found to be due to two separate aerosols arising in different time regimes after firing. Obscuration is initially attributed to a water-based gun smoke aerosol of 1.0-1.5$\mu$m particles followed in 3 to 6 seconds by a clay-based dust aerosol of 4-5$\mu$m particles rising from the ground. The evolution of each aerosol in terms of changing particle sizes and number densities is followed, and the interplay of absorption effects and scattering effects at various wavelengths is discussed.

## PREFACE

This study was conducted at Pitman-Dunn Laboratory, Frankford Arsenal, Philadelphia, Pennsylvania, under the sponsorship of the Fire Control Program. It covers work which was performed through August 1977 under Project 1T161102A71A.

The use of trade names in this report does not constitute an official endorsement or approval of the use of such commercial hardware or software. This report may not be cited for purposes of advertisement.

Reproduction of this document in whole or in part is prohibited except with permission of the Commander/Director, Chemical Systems Laboratory, Attn: DRDAR-CLJ-R, Aberdeen Proving Ground, Maryland 21010; however, DDC and the National Technical Information Service are authorized to reproduce the document for United States Government purposes.

## TABLE OF CONTENTS



## LIST OF ILLUSTRATIONS

## LIST OF TABLES

# THE NATURE OF GUN SMOKE AND DUST OBSCURATION DUE TO CANNON FIRING

## INTRODUCTION

Sophisticated future fire control systems have been proposed which track a fired projectile along its trajectory and sense the miss distance at the target for automatic correction. To be successful, the system must be able to optically track the projectile during the first few seconds after firing, during which time the transparency of the atmosphere near the muzzle is very seriously degraded by gun gases, gun smoke, and dust clouds created from the ground by muzzle blast. We here present an analysis of optical transmission data in three wavelength regions (visible, near IR, and far IR) collected for single shot firing of a Rarden 30 mm cannon, which results in a quantitative model for the gun smoke aerosol and for the dust aerosol responsible for the obscuration. The purpose of this study is to contribute data on obscuration effects which is required as part of an assessment of the relative potential of lasers operating at wavelengths of 0.53μm, 1.06μm, and 10.6μm for providing an active projectile tracking system. This study was sponsored by the Photoelectric Laboratory and by the Automatic Cannon Technology Fire Control Office of the Fire Control Development and Engineering Directorate, Frankford Arsenal.

## DATA RESOURCES

The optical transmission data on which this study is based were taken from a series of experiments conducted by Heater, Pontelandolfo, and McKeough[1] at Aberdeen Proving Ground during the summer of 1974. Each shot of the Rarden 30 mm cannon was filmed and optical transmission data were recorded for a path 93 feet long, parallel to the gun-target axis and passing alongside the muzzle. These radiometric measurements were made in two optical bands of 200 Å width centered about wavelengths of 0.53μm and 1.06μm, and in a third optical band of 0.22μm width centered about 10.6μm. The films of each shot were reviewed to select for analysis one with wind conditions as quiet as possible in order to avoid confounding intrinsic aerosol effects with transmission changes due to wind moving the aerosol cloud around in the optical path; in this way shot #3 was selected for detailed analysis. The data are shown in Figure 1.

The infrared transmission spectrum over a similar optical path was available for one of the other shots (#4). The data, as reduced from the Fourier transform spectrometer recording, are shown in Figure 2.

[1] J. McKeough and J. Heater, "Obscuration Measurements on 30 mm Rarden Gun", FA-TR-76037, Frankford Arsenal, Philadelphia, PA 19137 (July 1976).

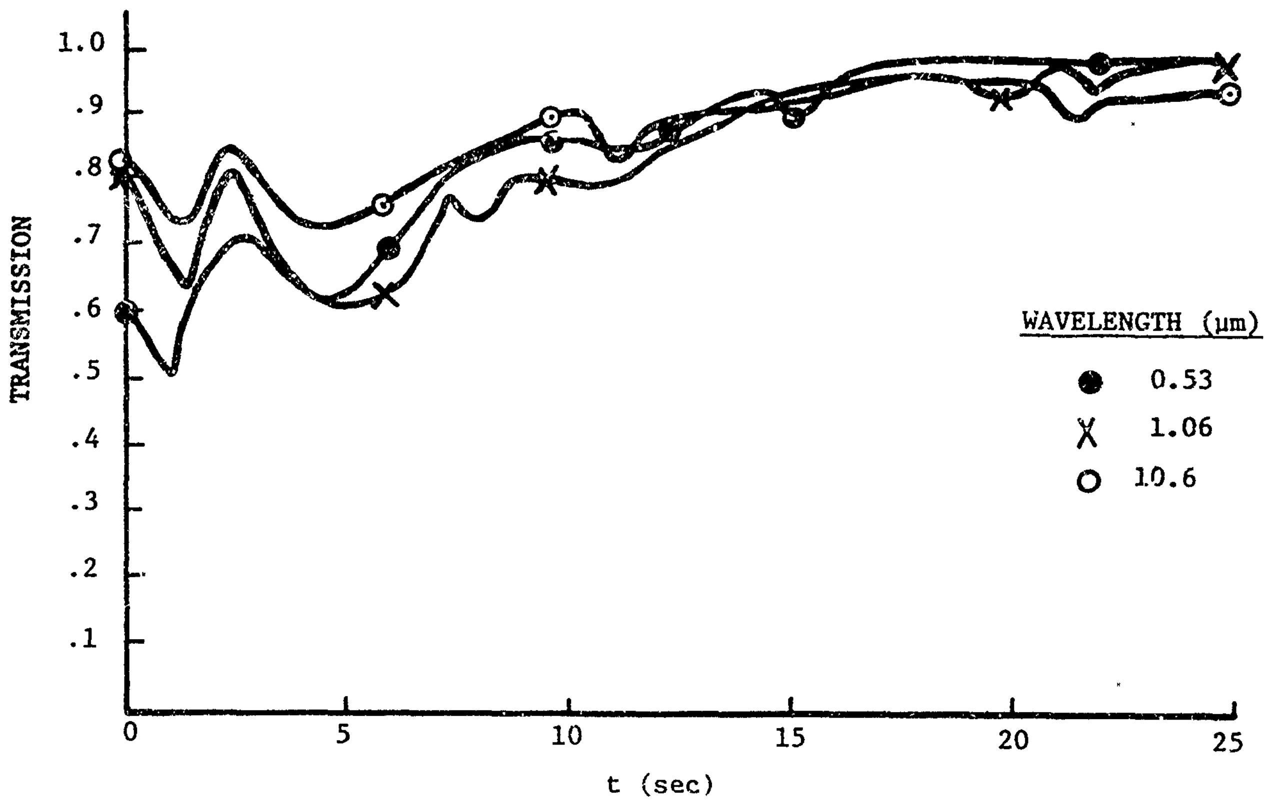


Figure 1. Transmission vs. Time (secs.) for Shot 3.

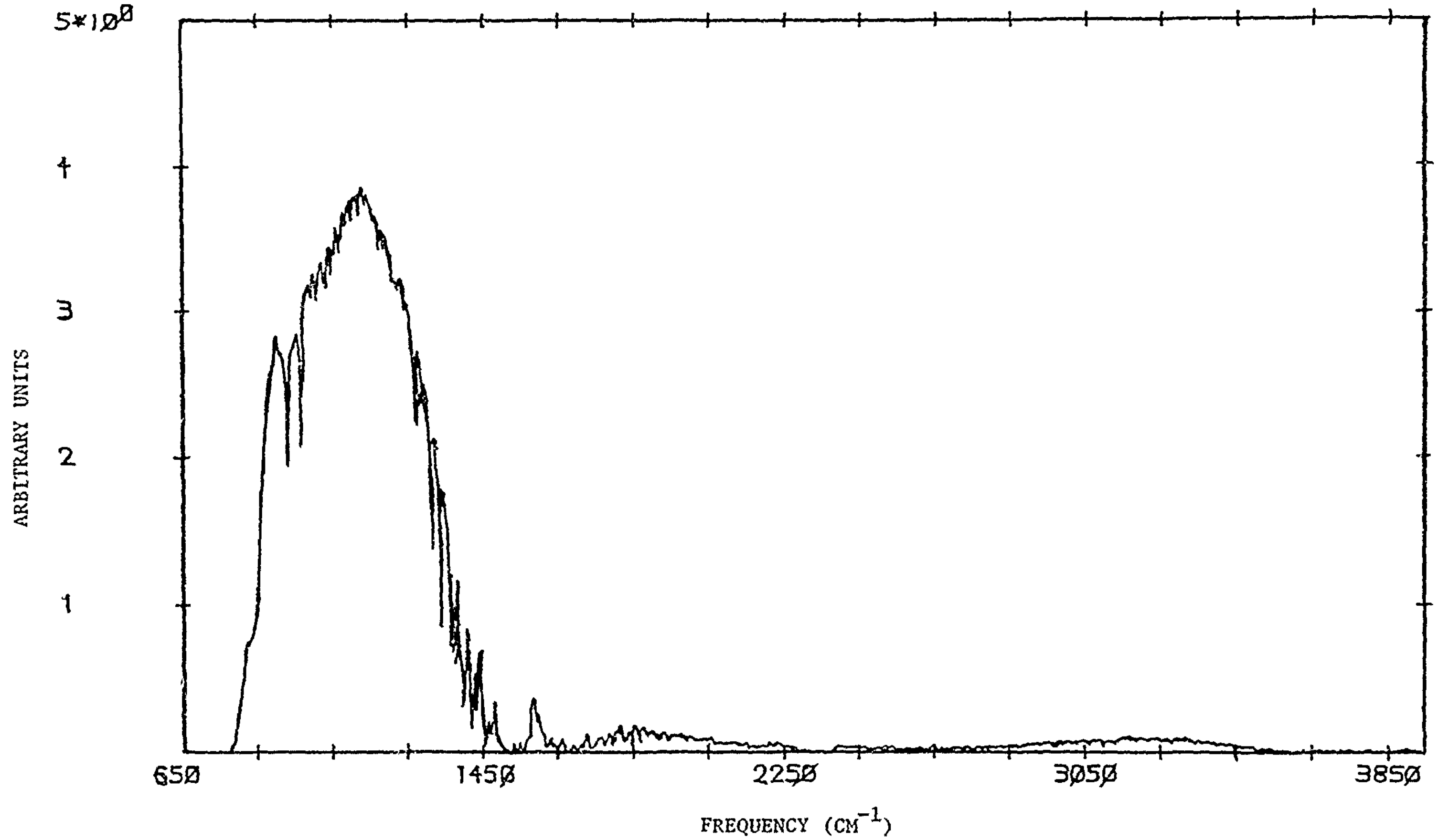


Figure 2. Infrared Spectrum of Gun Smoke and Gases.

The basic envelope of the peak in the 800-1450 $cm^{-1}$ region is the emission of the glowing coil source. The jagged absorption bands along the high wave number side of the envelope are due to water, the strong absorption doublet in the 900-100 $cm^{-1}$ region and nearby weaker bands are due to ammonia ($NH_3$). Following the decay of this doublet in time showed the time dependence of the $NH_3$ absorption which is plotted in Figure 3. This $NH_3$ absorption falls within the band pass of the 10.6μm radiometer, so that the presence of $NH_3$ in the muzzle gases will confound the optical data we would like to attribute to the aerosol. Because the spectrometer data were not available for shot #3, they cannot be related directly to the radiometer data of Figure 1; however, $NH_3$ absorption can be expected to interfere seriously with the validity of any inference on the aerosol based on 10.6μm radiometer data, especially during the first 2-3 seconds following the shot.

Samples of loose dirt were collected from the surface of the ground at three different locations near and forward of the muzzle by the experimental crew. These were made available to the authors for laboratory study.

## MODEL CONCEPT

The obscuration effect will be modeled as due to two aerosols: (1) gun smoke and (2) dust created from the ground by muzzle blast. In Figure 1, the general features at all three wavelengths show a transmission minimum at about 1 1/2 seconds, rising to a maximum at 2 1/2 seconds, followed by a second minimum at 4 seconds, and then gradually rising to well above 90% as the obscuration clears. Examination of the data for all shots[1] reveals that this double minimum (min-max-min) structure within 5 seconds, followed by relatively smooth restoration of visibility, is a common feature. Viewing the films of the shots shows that first a greyish-white smoke cloud forms in the air in front of the muzzle almost instantly on firing (it does not appear to issue from the muzzle as smoke, rather the smoke forms in the air), and second, the muzzle blast shock wave can be seen racing along the ground sweeping along a low-lying dust skirt which then rises in a swirling, turbulent cloud after the shock wave has passed. By timing the visible effect on the screen, this dust cloud appears to reach the optical path of the radiometers (about shoulder high) in 3 to 5 seconds after firing. This agrees in time with the appearance of the second transmission minimum.

[1] J. McKeough and J. Heater, "Obscuration Measurements on 30 mm Rarden Gun", FA-TR-76037, Frankford Arsenal, Philadelphia, PA 19137 (July 1976).

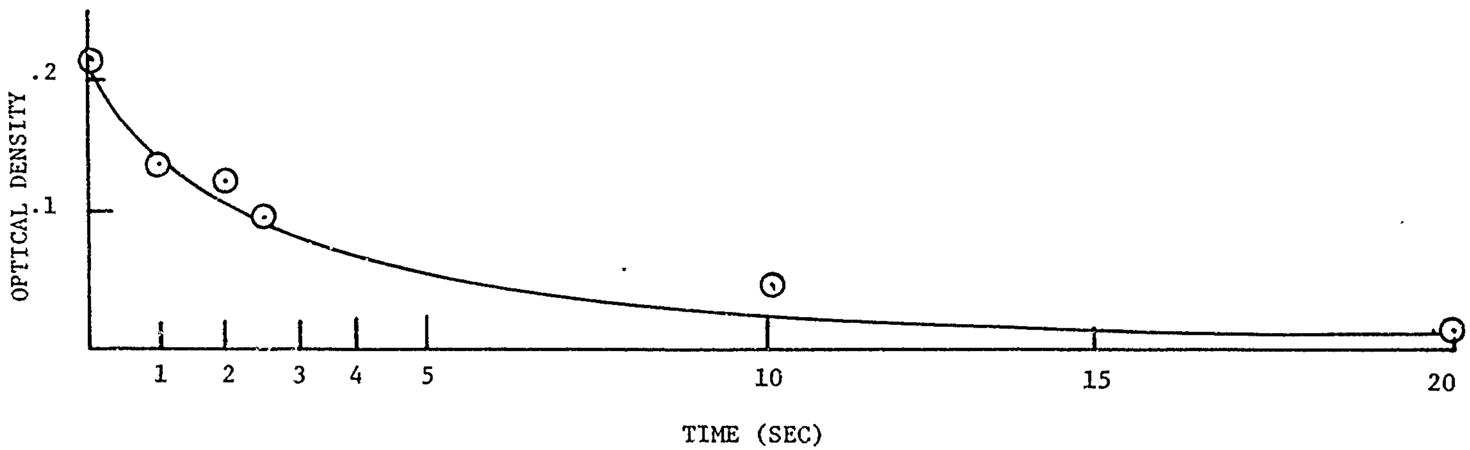


Figure 3. Optical Density Due to Ammonia as a Function of Time (Shot 4), $\nu$ = 930 $cm^{-1}$.

We propose then the following concept model. The initial obscuration is due to gun smoke which for reasons identified below increases in opacity for the first second or so and then dissipates. As the smoke cloud dissipates, the dust cloud rising from the ground enters the optical path resulting in increasing opacity for a while and then dissipates. The min-max-min transmission behavior is then attributed to smoke-dissipation-dust-dissipation. The following sections explore the detailed nature of these two aerosols based on the data for Shot #3 (Figure 1).

## APPROACH

In an extinguishing medium a light beam is attenuated according to

$$I = I_o e^{-\varepsilon C \ell} \tag{1}$$

where I is the transmitted intensity, $I_o$ is the incident intensity, $\varepsilon$ is an extinction coefficient, and C and $\ell$ are the concentration and path length in the medium in units appropriate to those used to specify $\varepsilon$. In aerosol studies C is commonly given as a number density in units of particles per $cm^3$ and $\ell$ is given in meters. The extinction coefficient $\varepsilon$ is then in units of $cm^3/m$ which is an area (i.e., $10^{-2}$ $cm^2$), and has a particular value for any given particle depending on its composition (refractive index) size, shape, and the wavelength of light incident on it. Assuming spherical particles, then from the wavelength, particle size, and refractive index the extinction cross-section ($C_{ext}$) may be calculated using the well known Mie theory.[2] In general the particle may be composed of a material which absorbs light at the wavelength of interest so that the observed extinction will be due to absorption as well as scattering. In this case the refractive index will be a complex number with an imaginary component related to the degree of absorption. Therefore, performing such calculations with accuracy will require knowing the real and imaginary components of the refractive index, at the wavelengths of interest, for the material of which the aerosol particles are composed.

The transmission (T) as reported in Figure 1 is the ratio of transmitted to incident light intensity. Then from Equation (1)

---

[2] E. W. Stuebing, J. J. Pinto (FA), and R. B. Gomez (Atmos. Sci. Lab), "PGAUSS-LT: A Program for Computing Optical Properties of Single Scattering Aerosol Clouds of Homogeneous Particles", FA-TM-75019, Frankford Arsenal, Philadelphia, PA 19137 (April 1975).

$$T = I/I_o = e^{-\varepsilon C\ell} \tag{2}$$

The transmission is not conveniently related to the parameters $\varepsilon$ and C which are directly related to the aerosols we wish to characterize. Therefore, the transmission data is digitized at 0.5 second intervals and converted to optical densities (OD)

$$OD = -\log T = (1/2.303)\varepsilon C\ell \tag{3}$$

which provide a more convenient linear relationship. The experiment is then analyzed by seeking model aerosols for which values of $\varepsilon$, C, and $\ell$ can be derived which will lead to OD vs. time curves in agreement with the data.

The approach may be summarized as follows. First, a candidate material for the aerosol particles is chosen and real and imaginary components for its refractive index are selected at each of the three wavelengths for which experimental data were collected. Second, a series of Mie scattering calculations are performed at each wavelength for spherical particles of this material at a variety of particle diameters. Third, an effective particle diameter in the cloud must be selected at each point in time. This is done by comparing the observed ratios of extinction at the various wavelengths [OD(0.53μm)/OD(1.06μm) and OD (0.53μm)/OD(10.6μm)] to the ratios predicted from the Mie calculation for the various sized particles. Because the amount of extinction depends strongly on the ratio of particle size to wavelength, this measure can be used as a sensitive indicator of particle size. Unfortunately, it is not always unique to a single particle size, as we shall see. Finally, with $\varepsilon$ fixed by the choice of refractive index and the choice of particle size selected from the ratios of OD's at different wavelengths, the product $C\ell$ can be determined to agree with the magnitude of the observed extinction. For convenience in reporting we shall take the cloud to be unitform over the 93 foot path length and report C as an effective number density (units = $cm^{-3}$).

## SMOKE MODEL

The early obscuration phenomena including the first transmission minimum to the maximum at 2.5 seconds is to be attributed to gun smoke. As pointed out previously, the presence of significant amounts of $NH_3$ in the vicinity of the muzzle is to be expected during this time and confound the extinction data in the 10.6μm region. We shall, therefore, rely on the data at 0.53μm and 1.06μm in constructing the gun smoke model.

The presence of significant amounts of $NH_3$ is to be expected following the combustion of nitrocellulose base propellants. The products of nitrocellulose combustion are shown in Table I. The water gas reaction follows an equilibrium appropriate to the high temperature, high pressure conditions inside the bore as the projectile travels down the barrel. When the projectile exits from the muzzle there is a sudden, catastrophic loss of temperature and pressure which freezes the concentrations at essentially those typical of the in-bore high temperature, high-pressure environment. Under these conditions there is an equilibrium established between the $H_2$ in the water gas reaction, the $N_2$, and $NH_3$ which results in the observed significant concentrations of $NH_3$. Note that gaseous water will also be released and suddenly cooled as the projectile exits the muzzle. Also a variety of hygroscopic metals and metal oxides are present from propellant additives or primer mixes. These can be expected to form active condensation nuclei for the suddenly cooled water resulting from propellant combustion, and for atmospheric water in the vicinity of the muzzle. Water droplets are, therefore, selected as a model material for the gun smoke aerosol. This water is certainly contaminated with a variety of materials, however, without further data on chemical composition, it seems a reasonable first approximation to model the gun smoke as a pure water aerosol.

The results of Mie calculations on water drops are given in Table II. The complex indices of refraction at the wavelengths of interest are shown in the box. From the magnitude of the imaginary components it is clear that pure water has effectively no absorption at 0.53 and 1.06μm, and moderate absorption at 10.6μm. For various particle diameters, the optical density per particle/$cm^3$ per meter path length [cf., $\varepsilon$ in Equation (3)] is given for each wavelength along with the ratio of these extinctions at the two wavelengths of principal interest.

The development of the water aerosol model is shown in Table III. At each of the 0.5 second intervals, the observed ratio of extinction at the two wavelengths is shown. Referring to the theoretical results in Table II allows the identification of an effective particle diameter. Of course the actual aerosol will be polydisperse (i.e., have a distribution of particle sizes); we model it here in terms of an equivalent monodisperse aerosol. For example, at time zero the measurements show an OD at the 0.53μm wavelength 2.4 times greater than the OD at 1.06μm. Referring to Table II shows that for drops of pure water this ratio would be expected from drops 1.0μm in diameter. Then considering the absolute OD's actually observed at 0.53μm and 1.06μm and the cross sections $\varepsilon$ of a 1.0μm water drop at these two wavelengths, one finds from Equation (3) the required number density in the two cases to be $5.3 \times 10^3$ and $5.8 \times 10^3$, which are assigned as the range of uncertainty, and for the model a value of $5.6 \times 10^3$ is chosen. This process is repeated at each half second interval up to 2.5 seconds.

TABLE I. PRODUCTS OF NITROCELLULOSE COMBUSTION

Major Products

$CO$, $CO_2$, $H_2$, $H_2O$ (Water Gas Equilibrium)

$N_2$

Major Minor Products

$CH_4$, $NH_3$

Minor Minor Products

$C$, $K_2O$, $SnO_2$, $Na_2O$, $BaO$

(Pb, Sb, Si, Zr, Ca, Al)

| Wavelength | Refractive Index |
|---|---|
| 0.53 | 1.335 (1-0.000000001 ) |
| 1.06 | 1.325 (1-0.000000808 ) |
| 10.6 | 1.182 (1-0.06091 ) |

TABLE II. $H_2O$ CALCULATION

| DIAM. (μm) | OD/PART/METER 0.53 | 1.06 | 10.6 | OD 0.53 / OD 1.06 |
|---|---|---|---|---|
| 0.1 | 0.464(-10) | 0.282(-11) | 0.179(-10) | 16.5 |
| 0.5 | 0.150(-6) | 0.258(-7) | 0.225(-8) | 5.81 |
| 0.9 | 0.104(-5) | 0.367(-6) | 0.133(-7) | 2.83 |
| 1.0 | 0.134(-5) | 0.565(-6) | 0.183(-7) | 2.37 |
| 1.1 | 0.164(-5) | 0.824(-6) | 0.245(-7) | 1.99 |
| 1.2 | 0.182(-5) | 0.112(-5) | 0.320(-7) | 1.62 |
| 1.3 | 0.195(-5) | 0.150(-5) | 0.409(-7) | 1.30 |
| 1.4 | 0.210(-5) | 0.193(-5) | 0.517(-7) | 1.09 |
| 1.5 | 0.210(-5) | 0.238(-5) | 0.637(-7) | 0.88 |
| 1.6 | 0.195(-5) | 0.295(-5) | 0.778(-7) | 0.66 |
| 1.7 | 0.201(-5) | 0.351(-5) | 0.941(-7) | 0.57 |
| 1.8 | 0.215(-5) | 0.405(-5) | 0.113(-6) | 0.53 |
| 1.9 | 0.207(-5) | 0.475(-5) | 0.134(-6) | 0.44 |
| 2.0 | 0.233(-5) | 0.530(-5) | 0.157(-6) | 0.44 |
| 5.0 | 0.176(-4) | 0.220(-4) | 0.326(-5) | 0.80 |
| 10.0 | 0.687(-4) | 0.692(-4) | 0.332(-4) | 0.98 |
| 20.0 | 0.292(-3) | 0.278(-3) | 0.278(-3) | 1.05 |

TABLE III. WATER AEROSOL MODEL

| TIME | OBSERVED $\frac{OD(0.53)}{OD(1.06)}$ | DIAM. (μm) | $N_{H_2O}$ (UNITS = $10^3$) RANGE | MODEL |
|---|---|---|---|---|
| 0.0 | 2.4 | 1.0 | 5.3 - 5.8 | 5.6 |
| 0.5 | 2.1 | 1.1 | 5.3 - 5.4 | 5.4 |
| 1.0 | 1.7 | 1.2 | 5.4 - 5.6 | 5.5 |
| 1.5 | 1.1 | 1.4 | 3.4 - 3.6 | 3.5 |
| 2.0 | 1.2 | 1.35 | 2.8 - 2.9 | 2.8 |
| 2.5 | 1.1 | 1.4 | 1.4 - 2.3 | 1.8 |
| 3.0 | | 1.4 | | 1.2 |
| 3.5 | | 1.4 | | .85 |
| 4.0 | | 1.4 | | .60 |
| 4.5 | | 1.4 | | .42 |
| 5.0 | | 1.4 | | .29 |
| 6.0 | | 1.4 | | .20 |
| 7.0 | | 1.4 | | .07 |
| 8.0 | | 1.4 | | .034 |
| 9.0 | | 1.4 | | .017 |
| 10.0 | | 1.4 | | .008 |
| 15.0 | | 1.4 | | .002 |

Note that during the first 1 1/2 seconds the particle number density remains rather constant while the drops grow in size from 1.0 to 1.4μm. After this the drop size remains stable while the cloud dissipates.

After 2.5 seconds the effect of the rising dust aerosol dominates the observed extinction. Nevertheless, there remains a significant amount of water whose effect must be subtracted from the observed OD data in order to characterize the dust aerosol. A plot of $H_2O$ drop number density vs. time, Figure 4, shows that once droplet growth stops and the water cloud begins to dissipate, the reduction in log (N) appears to be quite linear as shown by the circled points. This trend was simply extrapolated, number density values read at successive 1/2 second intervals [triangles in Figure 4], and the droplets assumed to remain stabilized at 1.4μm diameter. The results are shown below the dotted line in Table III. Table II data then allows the calculation of remaining OD due to dissipating water at each wavelength.

The OD effects due to the final water model are shown in Figure 5, where the circled points show the experimental data, and crosses plot the effect contributed by the water model of Table III. The behavior at 0.53μm and 1.06μm is very well reproduced, with the exception of the point at 2.5 seconds. This is the cross-over point at the transition between a smoke-dominated cloud and a dust-dominated cloud; it would be reasonable to expect significant contributions from both aerosols here. As the model attempts to account for the effect entirely in terms of the smoke aerosol, it is not surprising that the agreement is less than perfect. Note also that this model cannot explain the observed obscuration at 10.6μm at all. In the context of our model concept this must be left to the effects of $NH_3$ gas absorption or contaminants which certainly must be present in the water. It seems unlikely that these water impurities would absorb significantly at the 0.53 and 1.06μm wavelengths because the cloud has no apparent color, therefore, the refractive index of the particles at these two wavelengths is not expected to differ greatly from that of pure water. Furthermore, the 1.0-1.4μm diameter particles are on the order of the same size as these two wavelengths, a condition which causes the extinction to be strongly dominated by scattering rather than absorption. On the other hand, 10.6μm radiation has a wavelength much longer than the particle size. This leads to considerably enhanced absorption in the overall extinction. If absorbing impurities are present in the water, they would be expected to most strongly affect the 10.6μm wavelength.

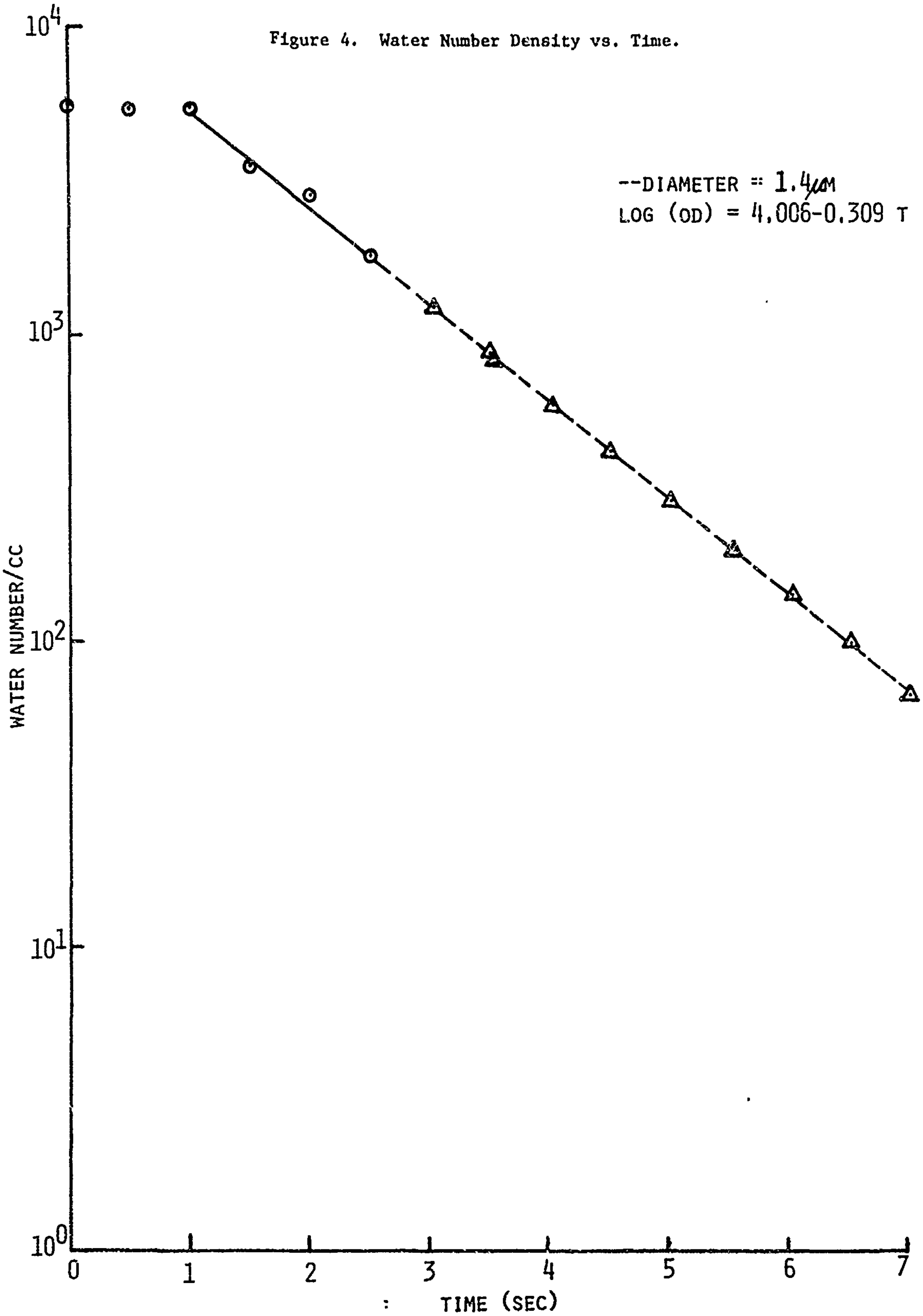

Figure 4. Water Number Density vs. Time.
--DIAMETER = 1.4μM
LOG (OD) = 4.006-0.309 T
WATER NUMBER/CC
$10^4$
$10^3$
$10^2$
$10^1$
$10^0$
0
1
2
3
4
5
6
7
TIME (SEC)

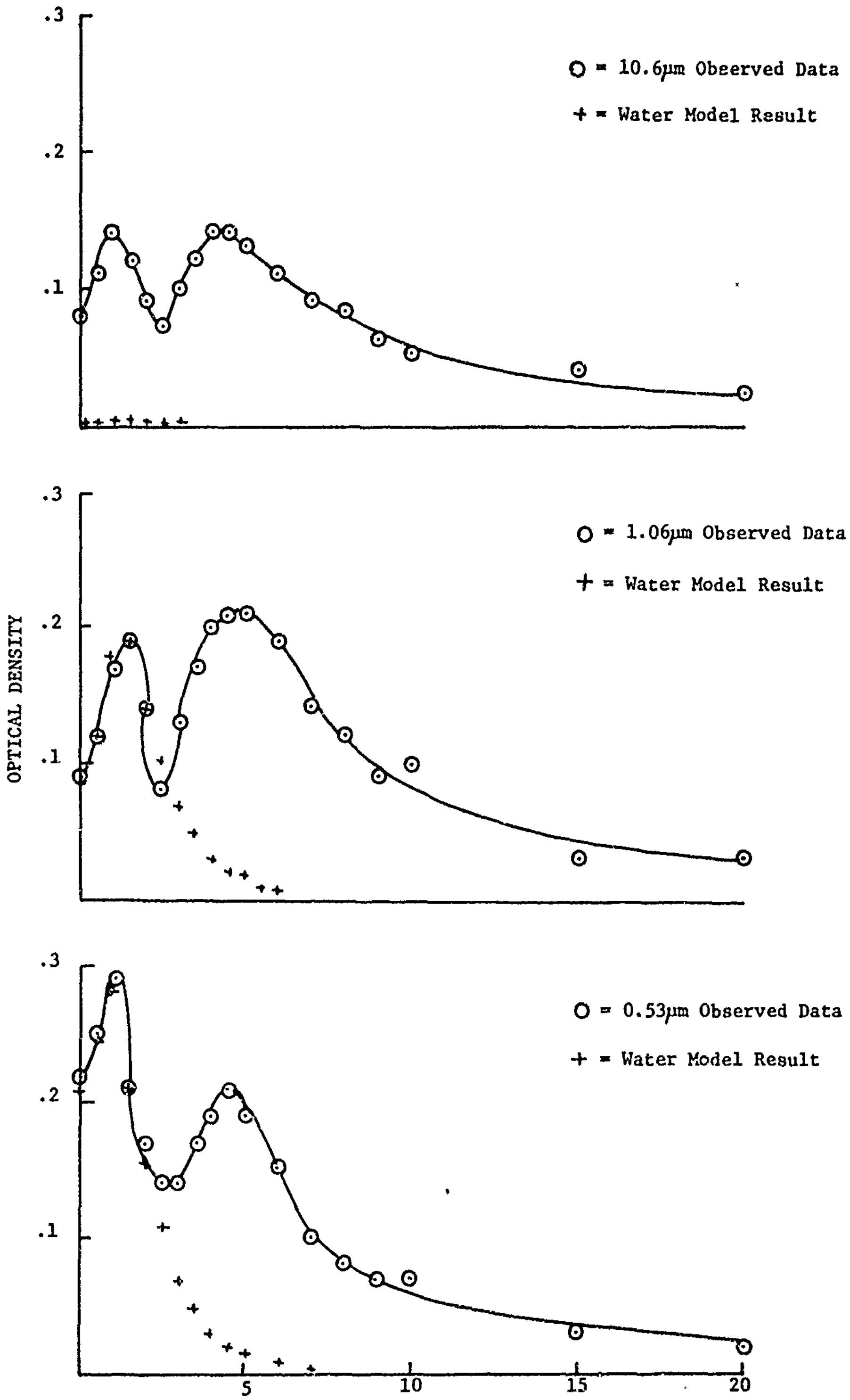


Figure 5. Optical Density Due to Gun Smoke Model.

## DUST MODEL

In order to establish a model refractive index for the dust particles comprising the aerosol, the dirt samples returned from the experiment site were examined. After sieving, the fines passing through a #320 mesh screen were mulled with KBr and pressed to form a pellet for spectroscopic study. The spectrum in the visible and infrared is shown in Figure 6. The KBr host is transparent in the visible; its IR spectrum is shown with that of the dust in order to sort out which features are to be attributed to the dust sample. In the visible, the smooth featureless increase in transmission with wavelength indicates: (1) only scattering processes are attenuating light in the sample, and (2) the particles responsible are not small compared to the wavelength because the increase is not sufficiently rapid (for very small particles compared to wavelength, Rayleigh scattering conditions obtain and the extinction follows $\lambda^{-4}$). The infrared spectrum shows a variety of absorption features. The infrared spectrum of a clay of known composition is shown in Figure 7 with the absorption features identified in terms of their origin on various components of the clay.[3] By comparison of the absorption features of Figures 6 and 7, it is clear that the dust sample is a clay.

From the literature, refractive index values typical of rural aerosols were taken for 0.53 and 1.06μm.[4] However, absorptions are expected to strongly influence extinction at the long 10.6μm wavelength, and clays of various compositions show absorptions at 10.6μm which vary over a wide range (greater than an order of magnitude). Therefore, in addition to a typical refractive index at 10.6μm[5], calculations were conducted for imaginary refractive index components at the lower and upper bounds expected for commonly occurring clays.[3] All of the refractive indices are given in Table IV.

[3] G. Hoidale, Atmospheric Sciences Laboratory, US Army Electronics Command, White Sands Missile Range, New Mexico, Private Communication.

[4] G. Hansel, "Computation of the Extinction of Visible Radiation by Atmospheric Aerosol Particles as a Function of the Relative Humidity, Based upon Measured Properties", Aerosol Sci. (1972).

[5] K. Fischer, "Bestimmung der Absorption von sichtbarer Strahlung durch Aerosolpartlikeln", Beitr. Phys. Atm. 43, p. 244 (1971).

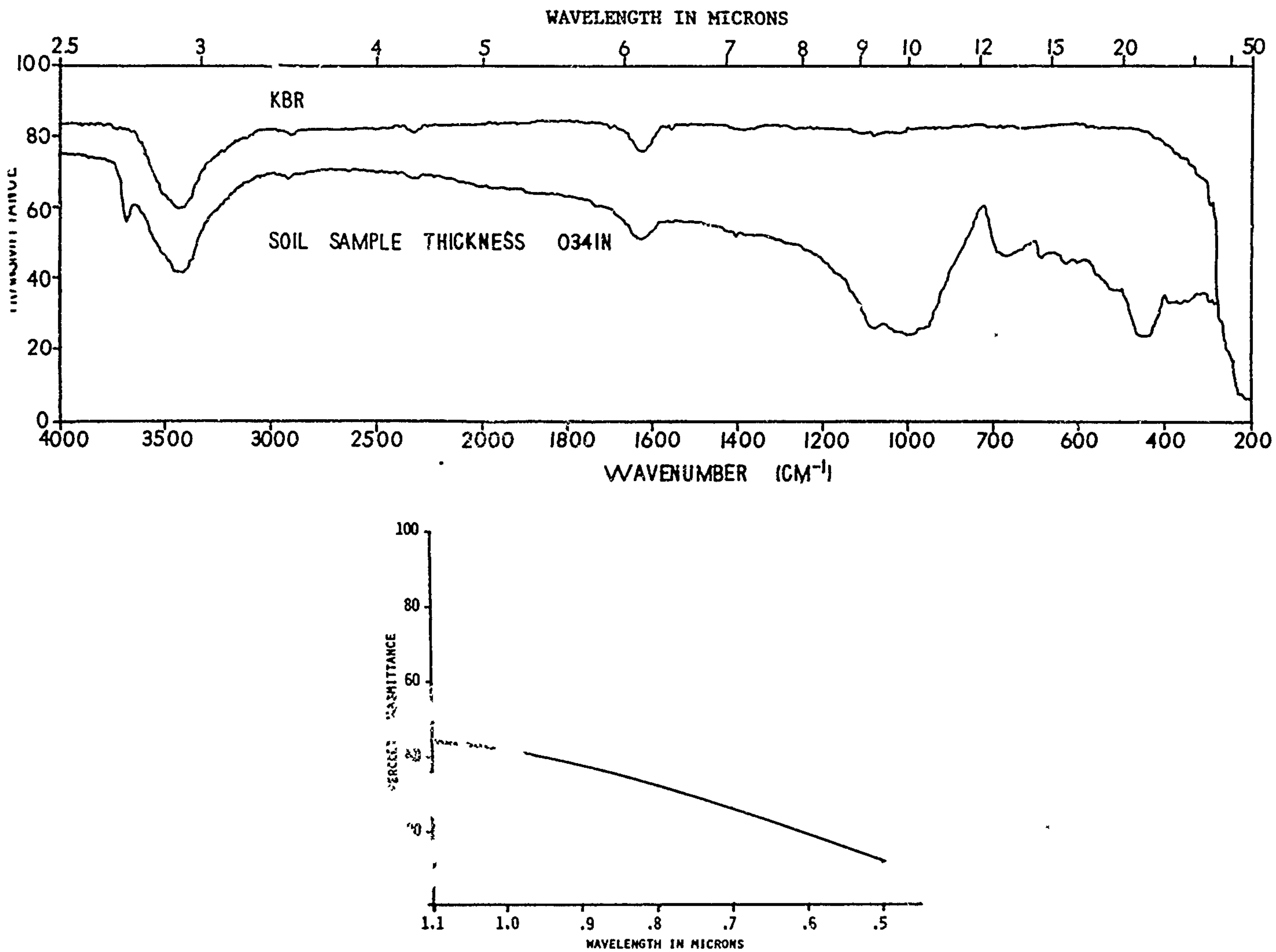


Figure 6. Visible and Infrared Spectrum of Dust Sample.

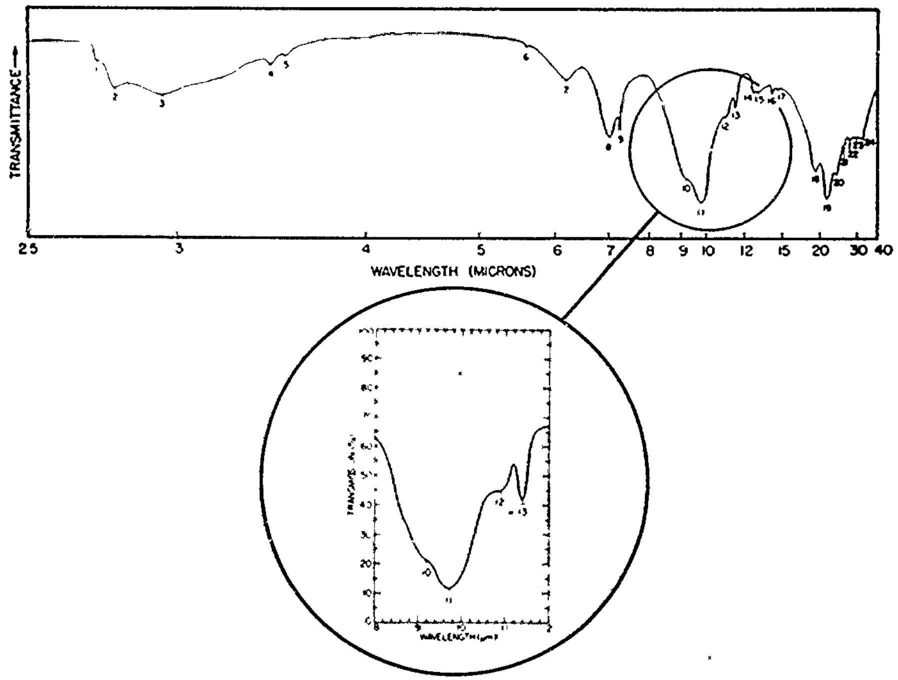


| BAND | λ(μm) | COMPONENT (S) |
|---|---|---|
| 1 | 2.7 | KAOLIN GROUP |
| 2 | 2.8 | KAOLIN GROUP |
| 3 | 2.9 | WATER (ABSORBED,ADSORBED) |
| 4 | 3.4 | HYDROCARBON |
| 5 | 3.5 | HYDROCARBON |
| 6 | 5.6 | CALCITE |
| 7 | 6.2 | WATER (ABSORBED, ADSORBED) |
| 8 | 7.0 | CARBONATE (MAINLY CALCITE) |
| 9 | 7.2 | NITRATE |
| 10 | 9.2 | QUARTZ, ILLITE, MONTMORILLONITE |
| 11 | 9.7 | ILLITE, MONTMORILLONITE, KAOLINITE |
| 12 | 10.9 | ILLITE, MONTMORILLONITE, KAOLINITE |

| BAND | λ(μm) | COMPOSITION (S) |
|---|---|---|
| 13 | 11.4 | CALCITE |
| 14 | 12.5 | QUARTZ, KAOLINITE |
| 15 | 12.9 | QUARTZ |
| 16 | 14.0 | CALCITE |
| 17 | 14.4 | QUARTZ, KAOLINITE |
| 18 | 19.2 | QUARTZ, ILLITE, MONTMORILLONITE, KAOLINITE |
| 19 | 21.4 | QUARTZ, ILLITE, MONTMORILLONITE, KAOLINITE |
| 20 | 23.1 | ILLITE, KAOLINITE |
| 21 | 25.3 | QUARTZ, KAOLINITE |
| 22 | 26.9 | QUARTZ, KAOLINITE |
| 23 | 29.2 | KAOLINITE |
| 24 | 31.7 | CALCITE |

| COMPONENT | ~% BY WEIGHT |
|---|---|
| MONTMORILLONITE | 35 |
| KAOLINITE | 20 |
| ILLITE | 20 |
| CALCITE | 15 |
| QUARTZ | 5 |
| OTHER | 5 |

Figure 7. Infrared Spectrum of Clay.

TABLE IV. MODEL REFRACTIVE INDICES FOR DUST

| WAVELENGTH (μm) | REFRACTIVE INDEX[a] |
|---|---|
| 0.53 | 1.51 (1.0 - 0.0093 ) |
| 1.06 | 1.49 (1.0 - 0.01342 ) |
| 10.6 (typical) | 1.67 (1.0 - 0.0808 ) |
| 10.6 (min) | 1.67 (1.0 - 0.0599 ) |
| 10.6 (max) | 1.67 (1.0 - 1.1078 ) |

[a]See text for identification of literature sources.

Mie calculations were performed at a variety of particle diameters and the ratios OD(0.53)/OD(1.06) and OD(0.53)/OD(10.6) constructed. These are tabulated in Table V. The listed values at 10.6μm are those for the typical refractive index, with the range of results for the minimum and maximum 10.6μm absorptions shown in parenthesis. The ratio OD(0.53)/OD(1.06) is an oscillating function of particle size, hence unique assignment of particle size based on this ratio alone is not possible. The ratio OD(0.53)/OD(10.6) is a monotonically decreasing function of particle size for fixed refractive index; furthermore, the range of values about the "typical" value is quite small for large particles (absorption has little effect as particles approach the wavelength in size) and grows to reflect the order of magnitude variation in imaginary refractive index component as absorption dominates extinction with particles small compared to the wavelength.

The experimental optical density data for 3.0 seconds and later were adjusted by subtracting the effect of the water model shown in Figure 5. The residual OD at each wavelength is then to be attributed to the dust aerosol. Ratios for this adjusted experimental data are shown in Table VI along with size and number density values characterizing two possible dust aerosol models to fit this data. At 3.0 seconds the ratio OD(0.53)/OD(1.06) from Table VI could be satisfied by particles of diameter 3.0μm or 5.0μm (of Table V). By 3.5 seconds, this ratio has dropped somewhat. Table V shows that this change in behavior could be accomodated at either 3 or 5μm particles and at both sizes this decrease in ratio could be accounted for by particles either growing or shrinking! Referring to the second ratio in Table VI [OD(0.53)/OD(10.6)] shows a consistent increase in this value between 3.0 and 5.0 seconds. Recalling the Table V monotonic theoretical

TABLE V. DUST IN AIR CALCULATION

| DIAM. (μm) | OD (0.53) / OD (1.06) | OD (0.53) / OD (10.6) |
|---|---|---|
| 1.1 | 0.69 | 27.3 (36.2 - 3.2) |
| 1.5 | 0.59 | 17.6 (22.7 - 2.0) |
| 2.0 | 0.87 | 11.0 (14.0 - 1.3) |
| 2.5 | 1.03 | 6.1 (7.4 - 0.82) |
| 3.0 | 1.08 | 4.4 (5.1 - 0.76) |
| 3.5 | 0.80 | 2.7 (3.1 - 0.66) |
| 4.0 | 0.89 | 2.1 (2.4 - 0.72) |
| 4.5 | 0.96 | 1.5 (1.6 - 0.67) |
| 5.0 | 1.07 | 1.25 (1.3 - 0.72) |
| 5.5 | 0.91 | 0.96 (0.98 - 0.66) |
| 6.0 | 0.92 | 0.90 (0.90 - 0.69) |
| 6.5 | 0.94 | 0.80 (0.79 - 0.67) |
| 7.0 | 1.04 | 0.77 (0.77 - 0.70) |

TABLE VI. CLAY AEROSOL MODEL

| TIME | DATA | | MODEL 1 | | MODEL 2 | |
|---|---|---|---|---|---|---|
| | OD(0.53)/OD(1.06) | OD(0.53)/OD(10.6) | DIAM. (μm) | N ($cm^{-3}$) | DIAM. (μm) | N ($cm^{-3}$) |
| 0.0 | | | | | | |
| 0.5 | | | | | | |
| 1.0 | | | | | | |
| 1.5 | | | | | | |
| 2.0 | | | | | | |
| 2.5 | | | | | | |
| 3.0 | 1.09 | 0.76 | 4.8 | 140 | 2.55 | 500 |
| 3.5 | 1.02 | 1.00 | 4.6 | 280 | 2.4 | 1075 |
| 4.0 | 0.95 | 1.17 | 4.5 | 380 | 2.35 | 1425 |
| 4.5 | 0.94 | 1.33 | 4.4 | 450 | 2.35 | 1640 |
| 5.0 | 0.89 | 1.35 | 4.1 | 480 | 2.1 | 1770 |
| 6.0 | 0.75 | 1.20 | | | 1.8 | [a] 1600 |
| 7.0 | 0.74 | 1.09 | | | 1.8 | 1170 |
| 8.0 | 0.63 | 1.00 | | | 1.8 | 1000 |
| 9.0 | 0.78 | 1.19 | | | 1.8 | 815 |

a. See text.

trend in this ratio for fixed refractive index (whatever the refractive index is for the particular Aberdeen dust, it is fixed in value), it is apparent that particle sizes are decreasing during this time.

Two possible models then explain the experimental data. One has dust particles of about 5μm diameter present at 3.0 seconds after firing with size diminishing thereafter; the second starts at particles of about 3μm and again reduces in size with time. This reduction in size with time is reasonable as the heavy particles will be the first to settle out of the dust cloud. Extensive Mie calculations to fill in data between the diameters shown in Table V lead to the assignment of particles sizes shown in Table VI. As with the water aerosol model, number densities are then calculated to provide the magnitude of obscuration observed. At 6.0 seconds and beyond, the obscuration curves at the various wavelengths come close together so that small variations (within experimental noise) cause them to cross and result in rather wild variations in the critical ratios. A reliable analysis of this data is not possible. For the 5μm model the OD(0.53)/OD(1.06) ratio cannot be matched; for the 3μm model this first ratio can be approximately satisfied by the 1.8μm diameter particles shown in Table VI, but these particles cannot match the OD(0.53)/OD(10.6) ratio even within the widest limits of reasonable 10.6μm absorption behavior (hence the dotted line flagging this data in Table VI is used to indicate unreliability). In general, the observed 10.6μm obscuration behavior falls closer to the middle of the range of expected refractive indices for the model using 5μm diameter particles than for the 3μm particle model which would require a clay composition of extremely strong absorption properties.

The three sieved dust samples returned to the laboratory were used to produce aerosols by shocking a container in which they rested and drawing the resulting dust cloud through a five-stage Battelle impactor for particle size analysis. The results for each of the three samples are shown in Table VII. The mean particle sizes agree with Model 1. As a check on the validity of the theoretical approach used in this study, each of these polydisperse aerosols from Table VII was used as the basis of a Mie calculation, the results of which were used to construct the ratios OD(0.53)/OD(1.06) for the separate polydispersions. Using each of these ratios to enter Table V, the predicted particle size for an equivalent monodisperse aerosol was found. These are shown in the last row of Table VII. The agreement with the actual mean particle sizes is remarkably good!

The final results of the clay dust model combined with the water smoke model are shown in Figure 8. At times of 3.0 seconds and greater the optical density due to water (crosses) and that due to clay (triangles) will add together to closely reproduce the experimental results at 0.53 and 1.06μm. At 10.6μm the range of results for the two

TABLE VII. PARTICLES SIZE COMPOSITION (%) FOR AEROSOLS PRODUCED FROM ABERDEEN PROVING GROUND CLAY SAMPLES

| PARTICLE DIAMETER ($\mu m$) | SAMPLE LOCATION MUZZLE | ROYCO | LAMP |
|---|---|---|---|
| 8 | 15.7 | 20.7 | 9.0 |
| 4 | 79.1 | 69.0 | 83.4 |
| 2 | 4.6 | 8.8 | 5.4 |
| 1 | 0.5 | 1.3 | 1.4 |
| 0.5 | 0.1 | 0.2 | 0.8 |
| TOTAL | 100 | 100 | 100 |
| | PARTICLE SIZE ($\mu m$) | | |
| Mean Particle Size | 4.5 | 4.6 | 4.2 |
| Equivalent Monodisperse[a] | 4.3 | 4.4 | 4.2 |

[a] See text

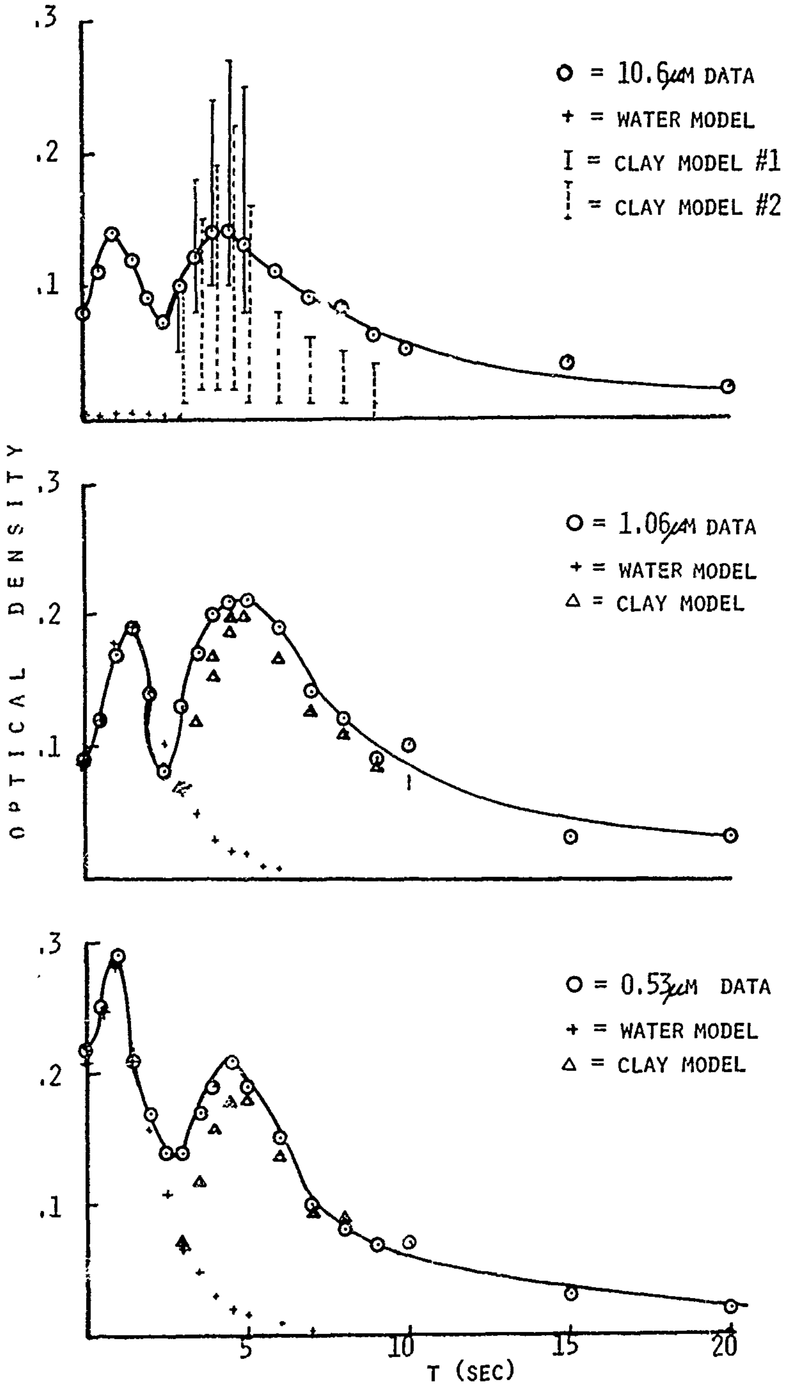


Figure 8. Optical Density Due to Gun Smoke and Dust Model.

clay models is indicated. The observed effects would be expected from a rather ordinary clay in Model 1; for Model 2 to be correct the clay would have to have been composed of an unusually strongly absorbing species. Because scattering strongly dominates the extinction at 0.53 and 1.06μm, and because the real components of the refractive indices of clays do not vary greatly, the observed extinction at these short wavelengths would be expected to be reasonably transferable to other geographical locations (types of clays). The indicated range of obscuration at 10.6μm can be read as suggesting the range of effects that might be found at other sites and hence suggests that "worst-case" conditions could result in twice the 10.6μm optical density observed during Aberdeen Proving Ground tests.

## SUMMARY

The obscuration due to single shot firing of the Rarden 30 mm cannon is modeled as resulting from two different monodisperse aerosols arising sequentially in time. The first aerosol, gun smoke, is composed of water drops condensed upon expansion of the water vapor product of propellant combustion and of atmospheric water vapor precipitated on condensation nuclei formed from propellant and primer combustion. This smoke cloud forms in front of the muzzle within a small fraction of a second after the projectile exits. Initially particles are spherical drops of about 1.0μm diameter which grow during the first second of time to 1.4μm without decrease in number density. As a result obscuration increases during this first second. Thereafter, particle size remains constant and dissipation of the aerosol results in decreased number density and obscuration. By three seconds, clay dust, which has been rising from the ground following the muzzle blast wave, begins to reach the height of the muzzle in quantities which produce more obscuration than the remaining smoke cloud. Particle diameter at three seconds is probably near 5μm, although it would be possible for particles of about half this size to also satisfy the optical data. In either case particle size decreases with time thereafter due to settling of the heavier particles. The rising dust cloud causes continuously increasing number density at the muzzle level during the period from three to six seconds; however, the effect of the concommitant decrease in particle size results in increasing obscuration only up until the fifth second, after which time visibility continuously improves as the cloud settles and dissipates.

These smoke and dust aerosol models agree well with the optical data at 0.53μm and 1.06μm wavelengths. In these cases, the obscuration is due to scattering which is a process not strongly dependent on wavelength. Therefore, the data gathered using radiometers with relatively

large band pass filters should also be representative of the effect that would have been observed had lasers operating at these wavelenghts been used. The 10.6μm wavelength effects are not due to the aerosols alone; there are significant gas absorptions in this region due to ammonia produced by propellant combustion. In addition, the gun smoke aerosol based on pure water cannot account for the observed 10.6μm effect. It must, therefore, be attributed to absorptions due to contaminations which are certainly present in the water or to the ammonia gas absorption. The ammonia absorption is a doublet falling almost entirely within the band pass of the radiometer; however, the 10.6μm wavelength itself falls on the high transmission spike between the absorption doublet. Therefore, the 10.6μm radiometer results are not expected to be typical of 10.6μm laser effects, the laser being expected to be superior in transmission, particularly during the first two seconds after firing.

Finally, unlike the results at wavelengths of 0.53 and 1.06μm, the 10.6μm wavelength results, even for aerosol effects, are due principally to absorption rather than scattering. This is particularly true of the dust obscuration, in which case the optical density can be expected to vary by a factor of three depending on the geographical location (i.e., chemical composition of the clay). The obscuration at 0.53 and 1.06μm wavelengths is due to scattering and is relatively insensitive to clay species or water impurities. Therefore, the 0.53μm and 1.06μm data is more likely transferable from location to location, with some dependence in the gun smoke expected on local conditions of relative humidity.

## REFERENCES


1. J. McKeough and J. Heater, "Obscuration Measurements on 30 mm Rarden Gun", FA-TR-76037, Frankford Arsenal, Philadelphia, PA 19137 (July 1976).

2. E. W. Stuebing, J. J. Pinto (FA), and R. B. Gomez (Atmos. Sci. Lab), "PGAUSS-LT: A Program for Computing Optical Properties of Single Scattering Aerosol Clouds of Homogeneous Particles" FA-TM-75019, Frankford Arsenal, Philadelphia, PA 19137 (April 1975).

3. G. Hoidale, Atmospheric Sciences Laboratory, US Army Electronics Command, White Sands Missile Range, New Mexico, Private Communication.

4. G. Hansel, "Computation of the Extinction of Visible Radiation by Atmospheric Aerosol Particles as a Function of the Relative Humidity, Based upon Measured Properties", Aerosol Sci. (1972).

5. K. Fischer, "Bestimmung der Absorption von sichtbarer Strahlung durch Aerosolpartlikeln", Beitr. Phys. Atm. 43, p. 244 (1971).

DISTRIBUTION LIST FOR ARCSL-TR-79050

| Names | Copies |
|---|---|
| Chemical Systems Laboratory | |
| Aberdeen Proving Ground, MD 21010 | |
| Office of the Director | |
| Attn: DRDAR-CLG | 1 |
| CB Detection & Alarms Division | |
| Attn: DRDAR-CLC | 1 |
| Developmental Support Division | |
| Attn: DRDAR-CLJ-L | 3 |
| Attn: DRDAR-CLJ-R | 3 |
| Attn: DRDAR-CLJ-M | 1 |
| Munitions Division | |
| Attn: DRDAR-CLN | 1 |
| Attn: DRDAR-CLN-S | 1 |
| Physical Protection Division | |
| Attn: DRDAR-CLW-P | 1 |
| Research Division | |
| Attn: DRDAR-CLB | 1 |
| Attn: DRDAR-CLB-B | 1 |
| Attn: DRDAR-CLB-P | 1 |
| Attn: DRDAR-CLB-T | 1 |
| Attn: DRDAR-CLB-PS (Mr. Vervier) | 1 |
| Attn: DRDAR-CLB-PS (Dr. Stuebing) | 1 |
| Attn: DRDAR-CLB-PS (Mr. Frickel) | 1 |
| Systems Development Division | |
| Attn: DRDAR-CLY-A | 1 |
| Attn: DRDAR-CLY-R | 6 |
| **DEPARTMENT OF DEFENSE** | |
| Administrator | |
| Defense Documentation Center | |
| Attn: Document Processing Division (DDC-DD) | 12 |
| Cameron Station | |
| Alexandria, VA 22314 | |
| Office of the Director | |
| Defense Research and Engineering | |
| Attn: Dr. T.C. Walsh, Rm 3D-1079 | 1 |
| Washington, DC 20310 | |
| Institute for Defense Analysis | |
| 400 Army-Navy Drive | |
| Attn: L. Biberman | 1 |
| Attn: R. E. Roberts | 1 |
| Arlington, VA 22202 | |
| Advanced Research Projects Agency | 1 |
| 1400 Wilson Boulevard | |
| Arlington, VA 22209 | |

| Names | Copies |
|---|---|
| **DEPARTMENT OF THE ARMY** | |
| Commander | |
| US Army Research Office – Durham | 1 |
| Box CM, Duke Station | |
| Durham, NC 27706 | |
| HQDA (DAMO-SSC) | 1 |
| HQDA (DAMA-ARZ, Dr. Verderame) | 1 |
| HQDA (DAMA-CSM-CM) | 1 |
| HQDA (DAMI-FIT) | 1 |
| WASH DC 20310 | |
| **US ARMY MATERIEL DEVELOPMENT AND READINESS COMMAND** | |
| Commander | |
| US Army Materiel Development and Readiness Command | |
| Attn: DRCDE-DM | 1 |
| Attn: DRCLDC | 1 |
| Attn: DRCMT | 1 |
| Attn: DRCSF-S | 1 |
| Attn: DRCDL (Mr. N. Klein) | 1 |
| Attn: DRCBI (COL Gearin) | 1 |
| Attn: DRCDMD-ST (Mr. T. Shirata) | 1 |
| 5001 Eisenhower Ave. | |
| Alexandria, VA 22333 | |
| Commander | |
| US Army Foreign Science & Technology Center | |
| Attn: DRXST-MT-2 | 1 |
| Attn: DRXST-CE (Mr. V. Rague) | 1 |
| 220 Seventh St., NE | |
| Charlottesville, VA 22901 | |
| Commander | |
| US Army Missile Command | |
| Redstone Scientific Information Center | |
| Attn: Chief, Documents | 1 |
| Attn: DRDMI-CGA (Dr. B. Fowler) | 1 |
| Attn: DRDMI-TE (Mr. H. Anderson) | 1 |
| Attn: DRDMI-KL (Dr. W. Wharton) | 1 |
| Redstone Arsenal, AL 35809 | |
| **US ARMY ARMAMENT RESEARCH AND DEVELOPMENT COMMAND** | |
| Commander | |
| US Army Armament Research and Development Command | |
| Attn: DRDAR-TSS | 5 |
| Dover, NJ 07801 | |
| **US ARMY ARMAMENT MATERIEL READINESS COMMAND** | |
| Commander | |
| US Army Armament Materiel Readiness Command | |
| Attn: DRSAR-ASN | 1 |
| Attn: DRSAR-PE | 1 |
| Rock Island, IL 61299 | |

DISTRIBUTION LIST FOR ARCSL-TR-79050 (Contd)

| Names | Copies |
|---|---|
| Commander<br>Harry Diamond Laboratories<br>Attn: DRXDO-RDC (Mr. D. Giglio)<br>2800 Powder Mill Road<br>Adelphi, MD 20783 | 1 |
| Chief, Office of Missile Electronic Warfare<br>US Army Electronic Warfare Laboratory<br>Attn: DRSEL-WLM-SE (Mr. K. Larson)<br>White Sands Missile Range, NM 88002 | 1 |
| Project Manager for Smoke/Obscurants<br>Attn: DRCP-SMK<br>Aberdeen Proving Ground, MD 21005 | 2 |
| Commander<br>Atmospheric Sciences Laboratory | |
| Attn: DRSEL-BR-AS-P | 1 |
| Attn: DRSEL-BR-MS-A (Dr. R. Gomez) | 1 |
| Attn: DRSEL-BL-AS-DP (Mr. J. Lindberg) | 1 |
| Attn: DRSEL-BL-SY (Mr. F. Horning)<br>White Sands Missile Range, NM 88002 | 1 |
| Director<br>US Army Materiel Systems Analysis Activity | |
| Attn: DRXSY-D (Dr. Fallin) | 1 |
| Attn: DRXSY-MP<br>Aberdeen Proving Ground, MD 21005 | 1 |
| Director<br>Night Vision Laboratories | |
| Attn: DRSEL-NV-VI (Mr. R. Moulton) | 1 |
| Attn: DRSEL-NV-VI (Mr. R. Bergemann)<br>Fort Belvoir, VA 23651 | 1 |
| US Army Mobility Equipment Research and Development Center<br>Attn: Code/DROME-RT (Mr. O. F. Kezer)<br>Fort Belvoir, VA 22060 | 1 |
| Commander<br>US Army Electronics Command | |
| Attn: DRSEL-CT-LG (Dr. R. G. Rohde) | 1 |
| Attn: DRSEL-CT-1 (Dr. R. G. Buser) | 1 |
| Attn: DRSEL-WL-S (Mr. J. Charlton)<br>Fort Monmouth, NJ 07703 | 1 |
| Director<br>US Army Ballistic Research Laboratories | |
| Attn: DRXBR-DL (Mr. T. Finnerty). | 1 |
| Attn: DRXBR-P (Mr. N. Gerri) | 1 |
| Attn: DRDAR-BLB (Mr. R. Reitz) | 1 |
| Attn: DRDAR-BLB (Mr. A. LaGrange)<br>Aberdeen Proving Ground, MD 21005 | 1 |
| CDR, APG | |
| Attn: STEAP-AD-R/RHA | 1 |
| Attn: STEAP-TL<br>Aberdeen Proving Ground, MD 21005 | 1 |
| Commander<br>US Army Test & Evaluation Command<br>Attn: DRSTE-FA<br>Aberdeen Proving Ground, MD 21005 | 1 |
| Commander<br>Dugway Proving Ground | |
| Attn: STEDP-PO | 1 |
| Attn: Technical Library, Docu Sec | 1 |
| Attn: STEDP-MT-DA-E | 1 |
| Attn: STEDP-MT (Dr. L. Salamon)<br>Dugway, UT 84022 | 1 |
| US ARMY TRAINING & DOCTRINE COMMAND | |
| Commandant<br>US Army Infantry School<br>Combat Support & Maintenance Dept<br>Attn: NBC Division<br>Fort Benning, GA 31905 | 1 |
| Commandant<br>US Army Missile & Munitions Center & School | |
| Attn: ATSK-CD-MD | 1 |
| Attn: ATSK-DT-MU-EOD<br>Redstone Arsenal, AL 35809 | 1 |
| Commander<br>US Army Logistics Center<br>Attn: ATCL-MM<br>Fort Lee, VA 23801 | 1 |
| Commander<br>HQ, USA TRADOC<br>Attn: ATCD-TEC (Dr. M. Pastel)<br>Fort Monroe, VA 23651 | 1 |
| Commander<br>US Army Ordnance & Chemical Center & School | |
| Attn: ATSL-CD-MS | 1 |
| Attn: ATSL-CD-MS (Dr. T. Welsh)<br>Aberdeen Proving Ground, MD 21005 | 1 |
| DEPARTMENT OF THE NAVY | |
| Commander<br>Naval Surface Weapons Center<br>Attn: Tech Lib & Info Svcs Br<br>White Oak Laboratory<br>Silver Spring, MD 20910 | 1 |
| Commander<br>Naval Intelligence Support Center<br>4301 Suitland Road<br>Washington, DC 20390 | 1 |
| Commander<br>Naval Surface Weapons Center<br>Dahlgren Laboratory<br>Attn: DX-21<br>Dahlgren, VA 22448 | 1 |

DISTRIBUTION LIST FOR ARCSL-TR-79050 (Contd)

| Names | Copies |
|---|---|
| Commander<br>Naval Weapons Center<br>Attn: Code 3311 (Dr. R. Bird)<br>Attn: Code 382 (Dr. P. St. Amand)<br>Attn: Code 3822 (Dr. Hindman)<br>China Lake, CA 93555 | <br><br>1<br>1<br>1 |
| Commanding Officer<br>Naval Weapons Support Center<br>Attn: Code 5041 (Mr. D. Johnson)<br>Attn: Code 5042 (Mr. C. Dinerman)<br>Crane, IN 47522 | <br><br>1<br>1 |
| Commander<br>Naval Research Laboratory<br>Attn: Code 5709 (Mr. W. E. Howell)<br>4555 Overlook Avenue, SW<br>Washington, DC 20375 | <br><br>1 |
| DEPARTMENT OF THE AIR FORCE | |
| HQ, Foreign Technology Division (AFSC)<br>Attn: PDRR<br>Wright-Patterson AFB, OH 45433 | 1 |
| Commander<br>Armament Development & Test Center<br>Attn: DLOSL (Technical Library)<br>Eglin AFB, FL 32542 | 1 |
| Commander<br>USEUCOM<br>Attn: ECJ-O/LTC James H. Alley<br>APO, NY 09128 | 1 |